Improving identification of valid depth estimates from gravity gradient data using curvature and geometry analysis

Joseph Barraud* discusses practical ways to analyze the results provided by curvature-based depth estimation from gravity gradient data which allow the interpreter to discriminate between reliable and spurious estimates.

The interpretation of potential field data is generally considered as being either qualitative or quantitative. An important factor in any modelling and interpretation exercise is the confidence of the interpreter in the data which is providing the piece of information required to achieve the objectives of the study. The assessment of this interpretational confidence was recently addressed by Aitken et al. (2013) who proposed a method to quantify data richness.

The confidence in an interpretation can also be increased by the use of objective methods for estimating the depth of causative bodies. Although the knowledge of density or susceptibility contrasts is not required, most methods are based on the assumption that the source corresponds to a certain type (line, horizontal sheet, vertical dyke, etc.) and that the source is two-dimensional, i.e., it has an infinite dimension in one or two specific directions (Pilkington and Keating, 2004). Large errors can be made by selecting the wrong type of source, but more subtle errors can arise from the finite dimensions of the real source, from complex shapes and from the presence of interfering neighbouring sources. Additionally, data noise can affect the accuracy of the depth estimates in two ways: the location of the source becomes less accurate and myriads of unwanted estimates are added to the resulting map.

Despite these problems, numerous automated techniques have been designed and can be applied on gridded data to quickly provide depth estimates for all the magnetic or gravity anomalies. This article focuses on the methods based on the curvature of special functions of the data that peak over sources. A classic example of a special function is the horizontal gradient magnitude (HGM) that is commonly used to locate the edges of causative bodies (Roest and Pilkington, 1993). Special functions have a universal form for a variety of isolated sources and the study by Phillips et al. (2007) describes the common theoretical framework that supports all the possibilities offered by this technique. Only a small subset of these possibilities is described here.

This article discusses practical ways to analyze the results provided by curvature-based depth estimation. This allows the interpreter to discriminate between reliable estimates and spurious ones. This classification is performed by using both the shape of the anomaly and the geometry of the presumed source. Although the calculations are restricted here to gravity anomalies, it is possible to apply the method to magnetic anomalies as well. The method is first tested on synthetic models, and then applied to gravity gradiometry data from a recent multi-client survey in Pennsylvania, USA.

Curvature-based depth estimation

The method makes use of a family of special functions that are defined at (x,y,z) for a source at (x_0,y_0,z_0) by:

$$S(x,y,z) = \frac{\alpha Z}{X^2+Y^2+Z^2} \quad (1)$$

	Special function	Geometry factor α
Infinite horizontal cylinder	g_z or $abs(g_z)$	$2\pi a^2\rho\gamma$ (mGal.m or $m^2.s^{-2}$)
Semi-infinite slab	$HGM(g_z) = \sqrt{\left(\frac{\partial g_z}{\partial x}\right)^2 + \left(\frac{\partial g_z}{\partial y}\right)^2}$	$2\rho\Delta h\gamma$(mGal or $m.s^{-2}$)
Vertical contact	HGM of vertical derivative of g_z	$2\rho\gamma$ (mGal.m^{-1}or s^{-2})

Table 1 *Special function and geometry factor α for three gravity sources. For the cylinder, a is the radius (m), Δh is the thickness of the slab (m), ρ is the excess density (kg/m³), and γ is the gravitational constant (6.67×10^{-11} $m^3.kg^{-1}.s^{-2}$).*

**ARKeX. E-mail: joseph.barraud@arkex.com*

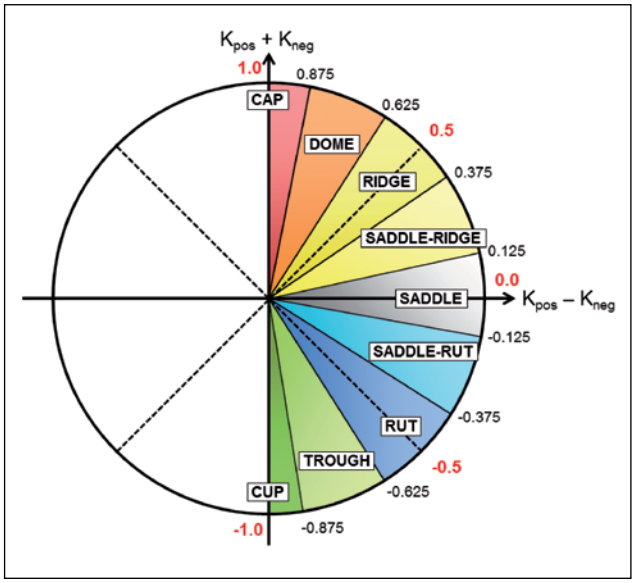

Figure 1 *Illustration of the Shape Index (SI) as an angle in the* $(K_{pos} - K_{neg}) \times (K_{pos} + K_{neg})$ *plane.*

where $X=(x-x_0)$, $Y=(y-y_0)$, $Z=(z-z_0)$, and α is a model-dependent geometry factor (Table 1). A special function is obtained by applying (or not) a transformation to the gravity anomaly produced by the source. The transformation depends on the type of source and, for example, would be the absolute value for a horizontal density line (or cylinder), or the horizontal gradient magnitude (HGM) in the case of the edge of a horizontal density sheet (Table 1). The basic idea is therefore to transform the gravity data into a surface that displays ridges directly over the assumed sources of the gravity field. The curvature of this surface in the (x,z)-plane is:

$$K(x,z) = \frac{\partial^2 S/\partial x^2}{[1+(\partial S/\partial x)^2]^{3/2}} \quad (2)$$

So for an elongated source lying parallel to the y axis, the curvature becomes at the peak:

$$K(x_0,z) = \frac{-2\alpha}{Z^3} = \frac{-2S(x_0,y_0,z)}{Z^2} \quad (3)$$

Therefore the depth of the source from the observation point is given by:

$$Z = \sqrt{-\frac{2S(x_0,y_0,z)}{K(x_0,z)}} \quad (4)$$

The depth is independent of the geometry factor and thus of the density contrast between the source and the surrounding medium. In other words, for simple geometric sources, the depth can be derived from the ratio between the amplitude and the curvature of the anomaly, or of a transformed version of the anomaly. The curvature is fundamentally a 2D concept that normally applies to curves or profiles.The curvature of a surface is only defined in terms of the curvature of a path that is taken across the surface. Moreover, the magnitude of the surface curvature will depend on the direction of the path. In order to apply equation (4) successfully, two assumptions have to be made: (1) the source is '2D' and has at least one infinite dimension (except for point sources), and (2) the curvature is calculated in a direction that is perpendicular to the direction of infinite dimension. Fortunately, the curvature analysis

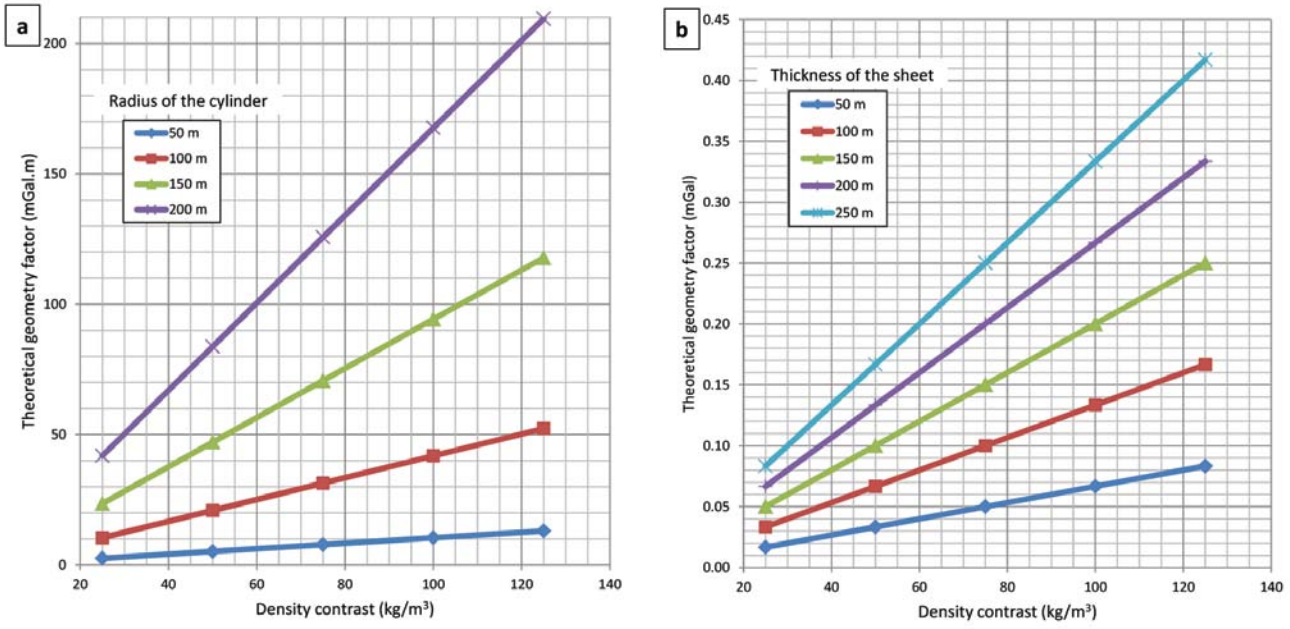

Figure 2 *Theoretical geometry factor as a function of density contrast.(a) horizontal cylinder; (b) thin sheet.*

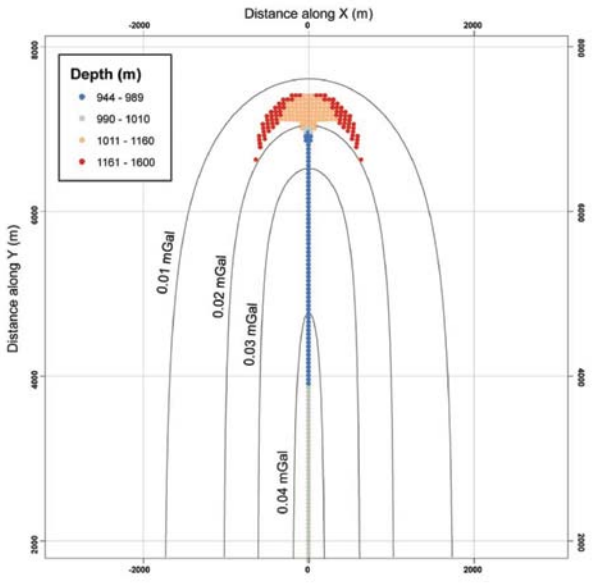

Figure 3 *Depth estimates for a horizontal cylinder of finite length (14 km) and radius 100 m buried at a depth of 1 km below the observation points. The excess density is +100 kg/m³. The plot only shows the northern half of the gravity anomaly. Depth estimates are plotted with points coloured as a function of depth.*

that follows provides a way to assess if these conditions are respected.

The implementation of the method for gridded data requires locating the ridges of the function S by passing a 3×3 window over the grid and fitting a quadratic surface through the nine points of the window (Roberts, 2001; Hansen and deRidder, 2006). The computation provides a series of attributes of the surface S, including the most negative curvature, K_{neg}, and the most positive curvature K_{pos} (Roberts, 2001). The magnitude of K_{neg} relative to K_{pos} is used to determine the concavity of the surface, whether it is a ridge or a trough (Phillips et al., 2007). Additionally, in the case of a ridge, K_{pos} is associated with a vector pointing in the direction of elongation of the quadratic surface. The curvature K_{neg} is therefore associated with the direction that is perpendicular to the source strike and is suitable for the calculation of depth with equation (4).

The quality of depth estimates can be assessed by calculating the Shape Index (Koenderink and van Doorn, 1992):

$$SI = \frac{2}{\pi}\tan^{-1}\left(\frac{K_{pos}+K_{neg}}{K_{neg}-K_{pos}}\right) \qquad (5)$$

By definition, K_{pos} is always greater than K_{neg}. Moreover, in this implementation, the curvature is negative for convex shapes, i.e., both K_{pos} and K_{neg} are negative for dome-like surfaces. SI ranges between –1 and +1, and can be seen as an angle in the $(K_{pos}- K_{neg})\times(K_{pos}+ K_{neg})$ plane (Figure 1). SI provides a convenient classification of shapes, going from the spherical cup (SI = –1) to the spherical convex cap

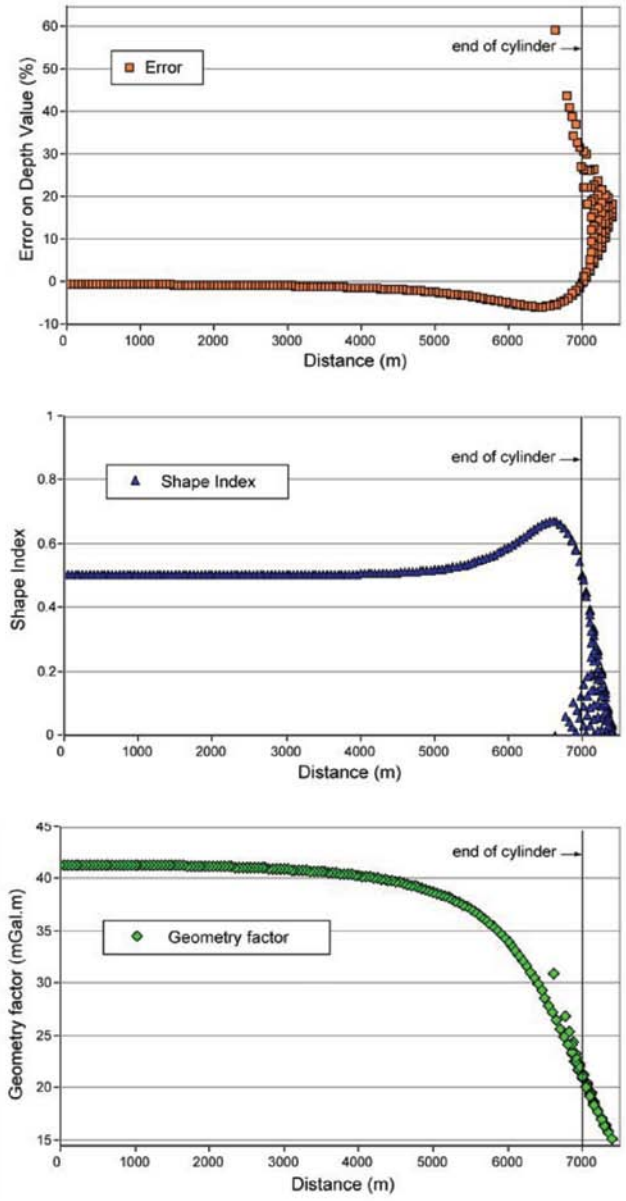

Figure 4 *Depth estimates for a horizontal cylinder as defined in Figure 3. The error on the calculated depth, the Shape Index and the calculated geometry factor are plotted against the distance along the y axis. The northern end of the cylinder is at y = 7 km.*

(SI = +1). SI is well suited to determine if the underlying special function S is diverging from the analytical solution that assumes perfect 2D conditions. If S has locally the shape of a ridge (SI=+0.5), then the gravity anomaly is more likely to originate from an elongated source that can be considered as infinite from the observation point. Non-ideal sources will distort the ideal shape of S and the SI will diverge from the ideal values of +0.5. In the classification proposed by Koenderink and van Doorn (1992), shapes with a SI comprised between 0.375 and 0.625 can still be considered as ridges (Figure 1).

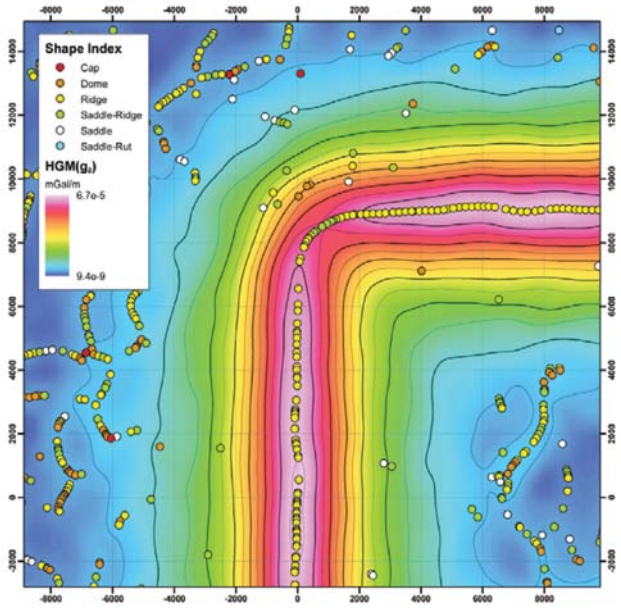

Figure 5 *Depth estimates for a semi-infinite slab of finite width (18 km in the y direction) and thickness 100 m lying flat at a depth of 1 km below the observation points. The excess density is +100 kg/m³. The contours of the HGM of g_z with noise added and upward continued by 1 km are shown for the northwest corner of the sheet only. Depth estimates are plotted as coloured dots depending on their associated Shape Index.*

Geometry factor

The geometry factor α theoretically depends on the density and on the dimensions of the source. It can also be calculated from the computed depth as follows:

$$\alpha = Z \times S(x_0, y_0, z) \tag{6}$$

By comparing the calculated value of α with the range of values expected in a given geological context, the number of incorrect points can be further reduced. The wrong type of source would also produce abnormal α values and can therefore be detected. The theoretical geometry factors for a thin sheet and a cylinder are plotted in Figure 2 for a typical range of the density values.

Examples with synthetic models

The method is first applied to the gravity anomaly produced by a cylinder of finite length parallel to the y axis. This example will illustrate the test on the condition of two-dimensionality. The vertical component of the gravity field is given by (Stavrev and Reid, 2007):

$$g_z = \frac{\alpha}{2}(z - z_0)\frac{\frac{y_1 - y + r_1}{r_1}\frac{y_2 - y + r_2}{r_2}}{(y_1 - y + r_1)(y_2 - y + r_2)} \tag{7}$$

where y_1 and y_2 are the coordinates of the extremities of the cylinder, and $r_i = [(x - x_0)^2 + (y - y_i)^2 + (z - z_0)^2]^{1/2}$, $i = 1,2$. The depth estimates were calculated with the method described above (Figure 3). The resulting points lie directly above the cylinder except at the extremities where a large number of points are spread around the curved end of the anomaly.

By plotting the relative error on the calculated depth as a function of distance along the cylinder, the effects of the finite length can be observed (Figure 4): approaching the end of the cylinder the calculated depth starts to decrease (remaining within about 5% of the true value) and then increases sharply to erroneous values. The SI follows a similar behaviour: the value is constant and equal to the theoretical value of 0.5 from the middle of the cylinder at y=0 up to y≈5 km. It then increases

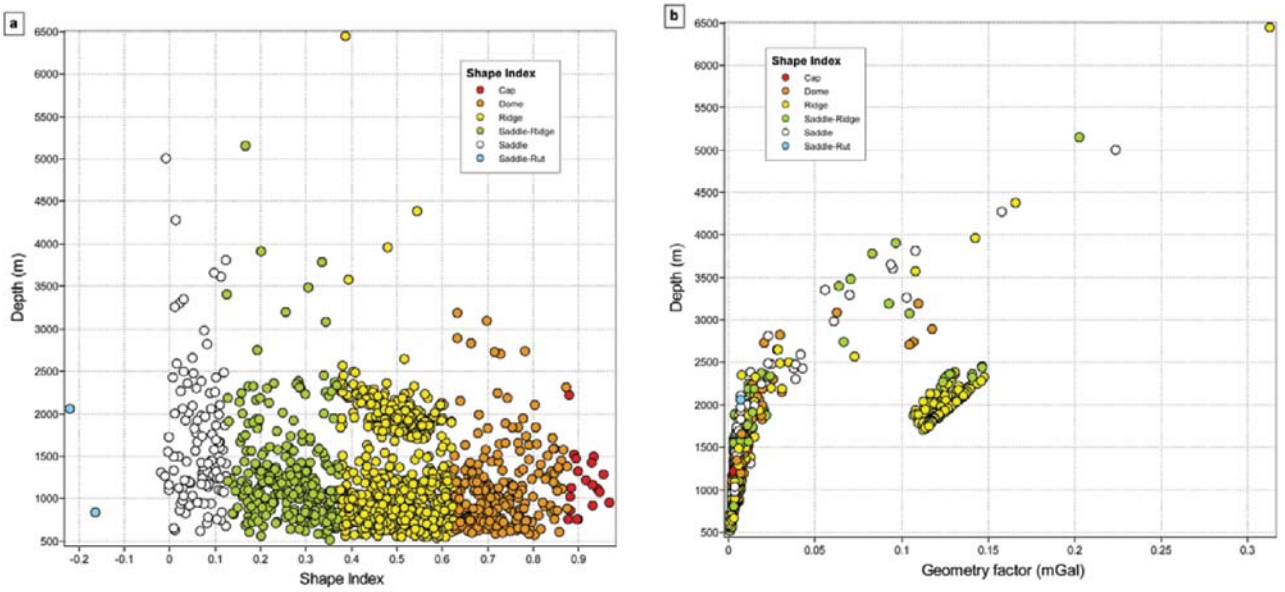

Figure 6 *Discrimination of depth estimates using the Shape Index and the geometry factor in the case of the thin sheet described in Figure 5. (a) Depth as a function of SI. The colours are the same as in Figure 5. (b) Depth as a function of the geometry factor. The source has a theoretical α value of 0.13 mGal. The correct depth is 2 km.*

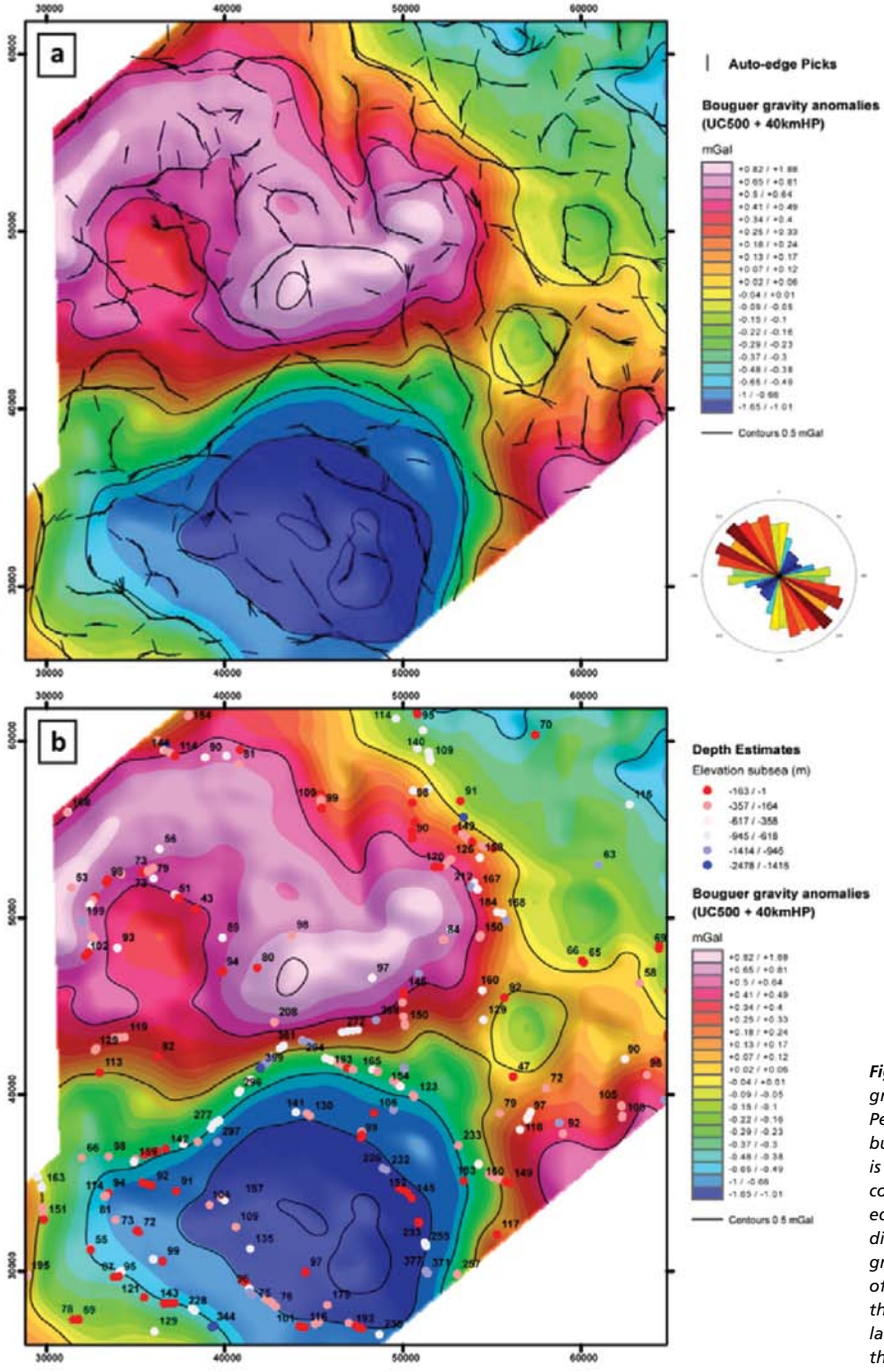

Figure 7 *Depth estimates calculated from ARKeX gravity gradiometry data acquired in western Pennsylvania. The coordinates have been modified but the scale has been preserved. Background data is g_z after terrain correction and filtering (upward continuation and high-pass filter). (a) The calculated points are displayed as sticks orientated in the direction of the strike of the anomaly. The rose diagram in the bottom-right corner gives a clear view of the main directions. (b) Depth estimates after the discrimination process (see text for details). The labels near the points indicate the calculated fault throw in metres.*

to about 0.67, showing that the shape of the anomaly locally becomes more dome-like than ridge-like. A sharp decrease of SI then follows, moving down the SI circle (Figure 1) from a dome back to a ridge, and then a saddle (SI=0) where the anomaly ultimately finishes.

This example shows that all the erroneous points can be rejected easily by selecting only the points with a SI value close to 0.5. The actual range of SI selected can be left to the appreciation of the interpreter depending on the quality of the data. This result also shows that the condition of dimensionality is satisfied to a reasonable degree even at a short distance from the end of the anomaly. Finally, the geometry factor is equal to the theoretical value (42 mGal.m) for all the points that can be picked with the SI criterion (Figure 4).

The effect of noise on the quality of depth estimates is investigated with the next example. The gravity anomaly produced by a semi-infinite slab of finite width was altered by the addition of white noise (standard deviation of 0.1 mGal).

The effect of the noise was then reduced by upward continuing the resulting data by 1 km. Depth estimates were calculated with the HGM special function and plotted on top of the grid (Figure 5). The presence of noise makes SI fluctuate around the ideal value of 0.5 along the edge of the sheet. By selecting only the points with a SI comprised between 0.375 and 0.625, a large number of incorrect estimates are discarded. Only 697 points out of 1362 are picked by the SI criterion (Figure 6a). However, many spurious points remain and a further selection is necessary. The plot of estimated depth versus calculated geometry factor shows a cluster of points around the theoretical values of α=0.13 mGal and depth=2000 m (Figure 6b). This is the correct depth after upward continuation and all the corresponding points are located around the edge of the thin sheet.

Example with real data

Airborne gravity gradiometry data were acquired by ARKeX during a multi-client survey in western Pennsylvania and eastern Ohio in 2012. Depth estimates were calculated in order to investigate the presence of faults at the levels of the Marcellus and Utica Shales, i.e., from about 0 to 2500 m below sea level. The source model is therefore the thin sheet and the special function is HGM applied to the gravity field. Gravity gradiometry offers a clear advantage for this type of study since the gravity gradients that are necessary to calculate HGM (G_{xz} and G_{yz}) are readily available.

Before calculating the depth estimates, an upward continuation of 500 m and a high-pass filter with a cut-off wavelength of 40 km were applied to the terrain-corrected gravity anomalies.This helps to reduce the interferences from sources above and below the specified target geology. The curvature-based method was then carried out as described above.

The first output of the tool is a map of auto-edge picks that shows the location and the strike of the anomaly edges, which can be a great aid for qualitative structural interpretation (Figure 7a).The SI values of these points were limited to the range 0.3 to 0.7, which is slightly larger than the range used for selecting depth estimates. This makes the picked edges more continuous.

The discrimination of depth estimates is now demonstrated in two stages. The results were first restricted to points with SI values between 0.375 and 0.625 and with elevation values (observation height minus calculated depth) smaller than zero (Figure 7b). About 3600 points were rejected by the selection process, leaving 758 points to plot. The resulting map is clearer because it only shows the estimates that could actually correspond to faults. The estimated value is theoretically the depth of the middle of the fault plane.

The geometry factor is used here in a different way: assuming a density contrast across the fault of 0.2 kg/m^3, the thickness of the corresponding slab was calculated with $\Delta h = \alpha/2\gamma\rho$ (Figure 7b). The interpreter can then compare this quantitative information with his knowledge of the local geology.

Discussion and conclusion

Despite its relatively simple theoretical background, a successful implementation of the depth estimation method depends on many parameters and mathematical techniques that can have an influence on the final results. The list comprises but is not limited to: the use of filtering or smoothing as pre-processing, the calculation of derivatives (using splines, convolution, or Fourier-domain techniques), the cell size of the grid, and the size of the window used for peak detection. The experience of the interpreter can play an important role at this stage in ensuring that meaningful results are present in the output.

The method of depth estimation based on the curvature of special functions is very suitable for an implementation in any GIS software, or as a Geosoft executable that can be plugged in Oasis Montaj (Phillips, 2007). Once the points have been generated, a large number of attributes are associated with each depth estimate. GIS software is ideally suited for browsing this large amount of data because the quality of the solutions can be assessed visually by applying thresholds on the Shape Index, the geometry factor, or the estimated depth.

Maps and graphs showing all or only the selected points can easily be generated to help the interpreter to reject spurious points according to the survey target and the available geological or geophysical information. This discrimination process can have a drastic effect on the final number of valid depth estimates. Although this might seem as a diminution of the information content of the potential-field data, this is a reliable way to increase the confidence of the interpreter in making a correct interpretation.

References

Aitken, A. Holden, E. and Dentith, M. [2013] Semi automated quantification of the influence of data richness on confidence in the geologic interpretation of aeromagnetic maps. *Geophysics*, **78**(2), J1–J13.

Hansen, R.O. and DeRidder, E. [2006] Linear feature analysis for aeromagnetic data. *Geophysics*, **71**(6), L61–L67.

Koenderink, J. and van Doorn, A. [1992] Surface shape and curvature scales. *Image and Vision Computing*, **10**, 557–564.

Phillips, J.D. [2007] Geosoft eXecutables (GX's) developed by the U.S. Geological Survey, Version 2.0, with notes on GX Development from Fortran Code. USGS Open-File Report 2007–1355.

Phillips, J.D. Hansen, R.O. and Blakely, R.J. [2007] The use of curvature in potential-field interpretation. *Exploration Geophysics*, **38**, 111–119.

Pilkington, M. and Keating, P. [2004] Contact mapping from gridded magnetic data – a comparison oftechniques. *Exploration Geophysics*, **35**, 306–311.

Roberts, A. [2001] Curvature attributes and their application to 3D interpreted horizons. *First Break*, **19**(2), 85–100.

Roest, W.R. and Pilkington, M. [1993] Identifying remanent magnetization effects in magnetic data. *Geophysics*, **58**, 653–659.

Stavrev, P. and Reid, A. [2007] Degrees of homogeneity of potential fields and structural indices of Euler deconvolution. *Geophysics*, **72**, L1–L12.